

Semi-Coupled Two-Stream Fusion ConvNets for Action Recognition at Extremely Low Resolutions

Jiawei Chen, Jonathan Wu, Janusz Konrad, Prakash Ishwar

Boston University

{garychen, jonwu, jkonrad, pi}@bu.edu

Abstract

Deep convolutional neural networks (ConvNets) have been recently shown to attain state-of-the-art performance for action recognition on standard-resolution videos. However, less attention has been paid to recognition performance at extremely low resolutions (eLR) (e.g., 16 × 12 pixels). Reliable action recognition using eLR cameras would address privacy concerns in various application environments such as private homes, hospitals, nursing/rehabilitation facilities, etc. In this paper, we propose a semi-coupled filter-sharing network that leverages high-resolution (HR) videos during training in order to assist an eLR ConvNet. We also study methods for fusing spatial and temporal ConvNets customized for eLR videos in order to take advantage of appearance and motion information. Our method outperforms state-of-the-art methods at extremely low resolutions on IXMAS (93.7%) and HMDB (29.2%) datasets.

1. Introduction

Human action and gesture recognition has received significant attention in computer vision and signal processing communities [21, 24, 29]. Recently, various ConvNet models have been applied in this context and achieved substantial performance gains over traditional methods that are based on hand-crafted features [9, 19]. Further improvements in the performance have been realized by using a two-stream ConvNet architecture [20], in which a spatial network concentrates on learning appearance features from RGB images and a temporal network takes optical flow snippets as input to learn dynamics. The final decision is made by averaging outputs of the two networks. More recent work [5, 11, 15] suggests fusion of spatial and temporal cues at an earlier stage so the appearance features are registered with motion features before the final decision. Results indicate that this approach improves action recognition performance.

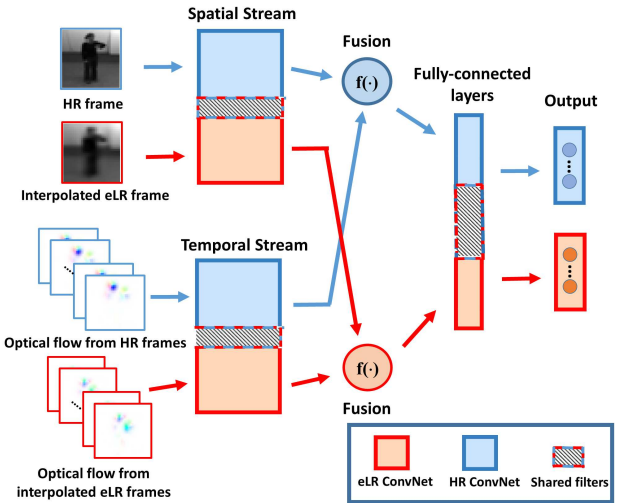


Figure 1: Diagram of the proposed ConvNet architecture. The blue blocks represent training-only HR information. The red blocks represent both training and testing eLR information. The overlap between the red and blue blocks indicates shared filters between eLR and HR information. Please note that both blocks use RGB and optical flow information.

As promising as these recent ConvNet-based models are, they typically rely upon data at about 200×200 -pixel resolution that is likely to reveal an individual's identity. However, as more and more sensors are being deployed in our homes and offices, the concern for privacy only grows. Clearly, reliable methods for human activity analysis at privacy-preserving resolutions are urgently needed [2, 16].

Some of the early approaches to action recognition from eLR data use simple machine learning algorithms (e.g., nearest-neighbor classifier) [3] or leverage a ConvNet but only as an appearance feature extractor [17]. In very recent work [26], a partially-coupled super-resolution network (PCSRN) has been proposed for eLR image classification (not video). Basically, this network includes two

ConvNets sharing a number of filters at each convolutional layer. While the input to one ConvNet consists of eLR images only, the input to the other network is formed from the corresponding HR images. The shared filters are trained to learn a nonlinear mapping between the eLR and HR feature spaces. Although this model has been designed for image recognition tasks, its excellent performance suggests that filter sharing could perhaps also benefit action recognition (from video) at extremely low resolutions.

In this paper, we combine the ideas of eLR-HR coupling and of two-stream ConvNets to perform reliable action recognition at extremely low resolutions. In particular, we adapt an existing end-to-end two-stream fusion ConvNet to eLR action recognition. We provide an in-depth analysis of three fusion methods for spatio-temporal networks, and compare them experimentally on eLR video datasets. Furthermore, inspired by the PCSRN model, we propose a semi-coupled two-stream fusion ConvNet that leverages HR videos during training in order to help the eLR ConvNet obtain enhanced discriminative power by sharing filters between eLR and HR ConvNets (Fig.1). Tested on two public datasets, the proposed model outperforms state-of-the-art eLR action recognition methods thus justifying our approach.

2. Related Work

ConvNets have been recently applied to action recognition and quickly yielded state-of-the-art performance. In the quest for further gains, a key question is how to properly incorporate appearance and motion information in a ConvNet architecture. In [7, 8, 22], various 3D ConvNets were proposed to learn spatio-temporal features by stacking consecutive RGB frames in the input. In [20], a novel two-stream ConvNets architecture was proposed which learns two separate networks: one dedicated to spatial RGB information, and another dedicated to temporal optical flow information. The softmax outputs of these two networks are later combined together to provide a final “joint” decision. Following this pivotal work, many works have extended the two-stream architecture such that only a single, combined network is trained. In [11], bilinear fusion was proposed in which the last convolutional layers of both networks are combined using an outer-product and pooling. Similarly, in [15] multiplicative fusion was proposed, and in [5] 3D convolutional fusion was introduced (incorporating an additional temporal dimension). However, all these methods were applied to standard-resolution video, and have not, to the best of our knowledge, been applied in the eLR context.

There have been few works that have addressed eLR in the context of visual recognition. In [26], very low resolution networks were investigated in the context of eLR *image* recognition. The authors proposed to incorporate HR images in training to augment the learning process of the

network through filter sharing (PCSRN). In [3], eLR action recognition was first explored using l_1 nearest-neighbor classifiers to discriminate between action sequences. More recently, egocentric eLR activity recognition was explored in [17] where the authors introduced the paradigm of inverse super resolution (ISR) to learn the optimal set of transformation parameters from HR to eLR, and then generate multiple eLR videos from a single eLR video. Then they extracted a number of per-frame features including histogram of pixel intensities, histogram of oriented gradients (HOG) [4], histogram of optical flows (HOF) [1] and ConvNet features. To capture temporal changes, they used the Pooled Time Series (POT) feature representation [18] which is based on time series analysis. We benchmark our proposed methodologies against these last two works, and are able to show consistent recognition improvement.

3. Technical Approach

In this section, we propose two improvements to the two-stream architecture in the context of eLR. First, we explore methods to fuse the spatial and temporal networks, which allows a single network to amplify and leverage joint spatial and temporal features. Second, we propose using semi-coupled networks which leverages HR information in training to learn transferable features from HR to eLR, resembling domain adaptation, in both the spatial and temporal streams.

3.1. Fusion of the two-stream networks

Multiple works have extended two-stream ConvNets by combining the spatial and temporal cues such that only a single, combined network is trained [5, 11, 15]. This is most frequently done by fusing the outputs of the spatial and temporal network’s convolution layers with the purpose of learning a correspondence of activations at the same pixel location. In this section, we discuss three fusion methods that we explore and implement in the context of eLR.

In general, fusion is applied between a spatial ConvNet and a temporal ConvNet. A fusion function $f: f(\mathbf{x}_s^n, \mathbf{x}_t^n) \rightarrow \mathbf{y}^n$ fuses spatial features at the output of the n -th layer $\mathbf{x}_s^n \in \mathbb{R}^{H_s^n \times W_s^n \times D_s^n}$ and temporal features at the output of the n -th layer $\mathbf{x}_t^n \in \mathbb{R}^{H_t^n \times W_t^n \times D_t^n}$ to produce the output features $\mathbf{y}^n \in \mathbb{R}^{H_o^n \times W_o^n \times D_o^n}$, where H , W , and D represent the height, width and the number of channels respectively. For simplicity, we assume $H_o = H_s = H_t, W_o = W_s = W_t, D_s = D_t$. We discuss the fusion function for three possible operators:

Sum Fusion: Perhaps the simplest fusion strategy is to compute the summation of two feature maps at the same pixel location (i, j) and the same channel d :

$$\mathbf{y}^{n, \text{sum}}(i, j, d) = \mathbf{x}_s^n(i, j, d) + \mathbf{x}_t^n(i, j, d) \quad (1)$$

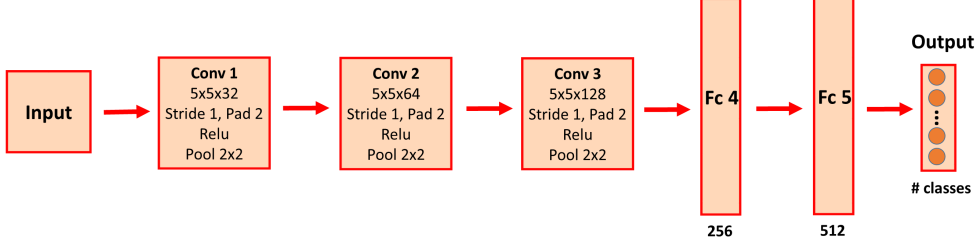


Figure 2: Basic ConvNet used in our model. The spatial and temporal streams have the same architecture except that the input dimension is larger in the temporal stream (the input to the temporal stream is a stacked optical flow). In our two-stream ConvNets, two base ConvNets are fused after either the “Conv3” or “Fc4” layer.

where $1 \leq i \leq H_o$, $1 \leq j \leq W_o$, $1 \leq d \leq D_o$ ($D_s = D_t = D_o$) and $\mathbf{x}_s^n, \mathbf{x}_t^n, \mathbf{y}^n \in \mathbb{R}^{H_o \times W_o \times D_o}$. The underlying assumption of summation fusion is that the spatial and temporal feature maps from the same channel will share similar contexts.

Concat Fusion: The second fusion method we consider is concatenation of two feature maps at the same spatial location (i, j) across channel d :

$$\mathbf{y}^{n,cat}(i, j, d) = \mathbf{x}_s^n(i, j, d), \mathbf{y}^{n,cat}(i, j, d+1) = \mathbf{x}_t^n(i, j, d) \quad (2)$$

where $\mathbf{y}^{n,cat} \in \mathbb{R}^{H_o \times W_o \times D_o}$, $D_o = D_s + D_t$. Unlike the summation fusion, the concatenation fusion does not actually blend the feature maps together.

Conv Fusion: The third fusion operator we explore is convolutional fusion. First, \mathbf{x}_s^n and \mathbf{x}_t^n are concatenated as shown in (2). Then, the stacked up feature map is convolved with a bank of filters $\mathcal{F} \in \mathbb{R}^{1 \times 1 \times D_o \times D'_o}$ as follows:

$$\mathbf{y}^{n,conv} = \mathbf{y}^{n,cat} * \mathcal{F} + b, \quad (3)$$

where $b \in \mathbb{R}^{D'_o}$ is a bias term. The filters have dimensions $1 \times 1 \times D_o$, $D_o = D_s + D_t$ and are used to learn weighted combinations of feature maps $\mathbf{x}_s^n, \mathbf{x}_t^n$ at a shared pixel location. For our experiments, we have set the number of filters to $D'_o = 0.5 \times D_o$.

Note, that regardless of the chosen fusion operator, the network will select filters throughout the entire network so as to minimize loss, and optimize recognition performance. Also, we would like to point out that other fusion operators, such as max, multiplication, and bilinear fusion [11], are possible, but have been shown in [5] to perform slightly worse than the operators we’ve discussed. Finally, it is worth noting that the type of fusion operation and the layer in which it occurs have a significant impact on the number of parameters. The number of parameters can be quite small if fusion across networks occurs in early layers. For example, convolutional fusion requires additional parameters since introducing a convolutional layer requires more filters. Regarding where to fuse the two networks, we adopt

the convention used in [5] to fuse the two networks after their last convolutional layer (see Fig. 3). We later report the results of fusion after the last convolutional layer and the first fully-connected layer (Conv3, Fc4) and contrast their classification performance.

3.2. Semi-coupled networks

Applying recognition directly to eLR video is not robust as visual features tend to carry little information [26]. Although only eLR videos are used in testing, it is possible to augment ConvNet training with an auxiliary, HR version of the eLR video. In this context, we propose to use semi-coupled networks which share filters between an eLR and an HR fused two-stream ConvNet. The eLR two-stream ConvNet takes an eLR RGB frame and its corresponding eLR optical flow frames as input. As we will discuss later, each RGB frame corresponds to multiple optical flows. The eLR RGB frames are interpolated to 32×32 pixels from their original 16×12 resolution. The eLR optical flow is computed across the upscaled eLR RGB frames of resolution 32×32 . The HR two-stream ConvNet simply takes HR RGB and its corresponding HR optical flow frames of size 32×32 as input. In layer number n of the network ($n = 1, \dots, 5$), the eLR and HR two-stream ConvNets share k^n filters. During training, we leverage both eLR and HR information, and update the filter weights of both networks in tandem. During testing, we decouple these two networks and only use the eLR network which includes shared filters. This entire process is illustrated in Fig. 3.

The motivation for sharing filters is two-fold: first, sharing resembles domain adaptation, aiming to learn transferable features from the source domain (eLR images) to the target domain (HR images); second, sharing can be viewed as a form of data augmentation with respect to the original dataset, as the shared filters will see both low and high resolution images (doubling the number of training inputs). However, it is important to note that in practice, as shown in [13], the mapping between eLR and HR feature space is difficult to learn. As a result, the feature space map-

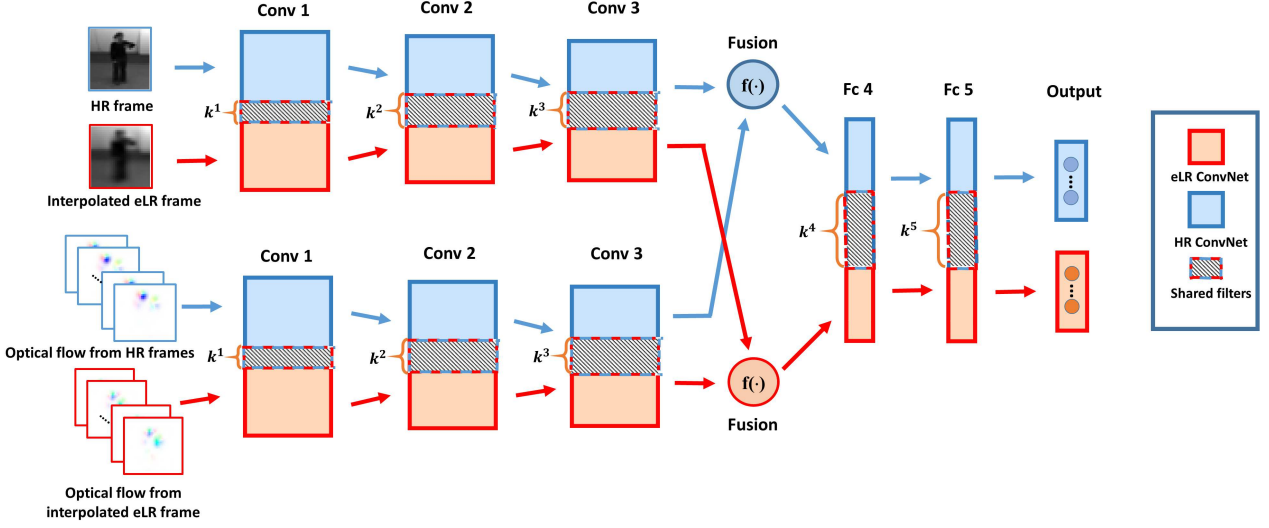


Figure 3: Visualization of the proposed semi-coupled networks of two fused two-stream ConvNets for video recognition. We feed HR RGB and optical flow frames (32×32 pixels) to the HR ConvNet (colored in blue). We feed eLR RGB (16×12 interpolated to 32×32 pixels) and optical flow frames (computed across interpolated 32×32 pixel RGB frames) to the eLR ConvNet (colored in red). In training, the two ConvNets share k^n ($n = 1, \dots, 5$) filters (gray shaded) between corresponding convolutional and fully connected layers. Note that the deeper the layer, the more filters are being shared. In testing, we decouple the two ConvNets and only use the eLR network (the red network which includes the shared filters).

ping between resolutions may not fully overlap or correspond properly to one-another after learning. To address this, we intentionally leave a number of filters ($D^n - k^n$) unshared in layer n , for each n . These unshared filters will learn domain-specific (resolution specific) features, while the shared filters learn the nonlinear transformations between spaces. To implement this filter sharing paradigm, we alternate between updating the eLR and HR two-stream ConvNets during training. Let θ_{eLR} and θ_{HR} denote the filter weights of the eLR and the HR two-stream ConvNets. These two filters are composed of three types of weights: θ_{shared} , the weights that are shared between both the eLR and HR networks, and θ_{eLR^*} , θ_{HR^*} , the weights that belong to only the eLR or the HR network, respectively. With these weights, we update both networks as follows:

$$\theta_{\text{eLR}}^m = \begin{bmatrix} \theta_{\text{eLR}^*}^{m-1} + \mu \frac{\partial L_{\text{eLR}}^{m-1}}{\partial \theta_{\text{eLR}^*}^{m-1}} \\ \theta_{\text{shared}}^{2m-2} + \mu \frac{\partial L_{\text{eLR}}^{m-1}}{\partial \theta_{\text{shared}}^{2m-2}} \end{bmatrix} \quad (4)$$

$$\theta_{\text{HR}}^m = \begin{bmatrix} \theta_{\text{HR}^*}^{m-1} + \mu \frac{\partial L_{\text{HR}}^{m-1}}{\partial \theta_{\text{HR}^*}^{m-1}} \\ \theta_{\text{shared}}^{2m-1} + \mu \frac{\partial L_{\text{HR}}^{m-1}}{\partial \theta_{\text{shared}}^{2m-1}} \end{bmatrix} \quad (5)$$

where μ is the learning rate, m is the training iteration, and L_{eLR} and L_{HR} are, respectively, the loss functions of each network. In each training iteration, the shared weights are updated in *both* the eLR and the HR ConvNet, i.e., they are updated twice in each iteration. Specifically, in each training iteration m , we have

$$\theta_{\text{shared}}^{2m-1} = \theta_{\text{shared}}^{2m-2} + \mu \frac{\partial L_{\text{eLR}}^{m-1}}{\partial \theta_{\text{shared}}^{2m-2}} \quad (6)$$

$$\theta_{\text{shared}}^{2m-2} = \theta_{\text{shared}}^{2m-3} + \mu \frac{\partial L_{\text{HR}}^{m-2}}{\partial \theta_{\text{shared}}^{2m-3}} \quad (7)$$

However, the resolution-specific unshared weights are only updated once: either in the eLR ConvNet training update or in the HR ConvNet training update. Therefore, the shared weights are updated twice as often as the unshared weights.

Our approach has been inspired by Partially-Coupled Super-Resolution Networks (PCSRN) [26] where it was shown that leveraging HR images in training of such networks can help discover discriminative features in eLR images that would otherwise have been overlooked during image classification. PCSRN is a super-resolution network that pre-trains network weights using filter sharing. This pre-training is intended to minimize the MSE of the output image and the target HR image via super-resolution. In our approach, we differ from this work by leveraging HR information throughout the *entire* training process. Our method

does not need to pre-train the network; instead, we learn the entire network from scratch, and minimize the classification loss function directly while still incorporating HR information as shown in the equations above. Overall, we extend this model in two aspects: first, we consider shared filters in the fully-connected layers (previously only convolutional layers were considered for filter sharing). Second, we adapt this method for action recognition in fused two-stream ConvNets. We also report results for semi-coupled two-stream ConvNets across various fusion operators.

3.3. Implementation details

Two-stream fusion network. Conventional standard-resolution ConvNet architectures can be ill-suited for eLR images due to large receptive fields that can sometimes be larger than the eLR image itself. To address this issue, we have designed an eLR ConvNet consisting of 3 convolutional layers, and 2 fully-connected layers as shown in Fig. 2. We base both our spatial and temporal streams on this ConvNet, and explore fusion operations after either the “Conv3” or “Fc4” layer. We train all networks from scratch using the Matconvnet toolbox [23]. The weights are initialized to be zero-mean Gaussian with a small standard deviation of 10^{-3} . The learning rate starts from 0.05 and is reduced by a factor of 10 after every 10 epochs. Weight decay and momentum are set to 0.0005 and 0.9 respectively. We use a batch size of 256 and perform batch normalization after each convolutional layer. At every iteration, we perform data augmentation by allowing a 0.5 probability that a given image in a batch is reflected across the vertical axis. Each RGB frame in the spatial stream will correspond to 11 stacked frames of optical flow. This stacked optical flow block will contain, the current, the 5 preceding, and 5 succeeding optical flow frames. To regularize these networks during training, we set the dropout ratio of both fully-connected layers to 0.85.

Semi-coupled ConvNets. In Section 3.2, we have discussed how to incorporate filter sharing in a semi-coupled network. However, it is not obvious how many filters should be shared in each layer. To discover the proper proportion of filters we should share, we conducted a coarse grid search for the coupling ratio c_n from 0 to 1 with a step size of 0.25. The coupling ratio is defined as:

$$c_n = \frac{k^n}{D^n}, \quad n = 1, \dots, 5 \quad (8)$$

where the two ConvNets are uncoupled when $c_n = 0$ ($n = 1, \dots, 5$). For the step sizes that we consider, a brute force approach would be unfeasible, as the total number of two-stream networks to train would be $5^5 = 3125$. Therefore, we follow the methodology used in [26] to monotonically increase the coupled ratios with increasing layer depth. This is inspired by the notion that the disparity between eLR and

HR domains is reduced as the layer gets deeper [6, 25]. For all our experiments, we used the following coupling ratios: $c_1 = 0$, $c_2 = 0.25$, $c_3 = 0.5$, $c_4 = 0.75$, and $c_5 = 1$. We determined these ratios by performing a coarse grid search on a cross-validated subset of the IXMAS dataset (subjects 2, 4, 6).

Normalization. In our experiments, we apply a variant of mean-variance normalization to each video $\{v_{i,j}[t], i, j = 1, \dots, R, t = 1, \dots, T\}$, where R is the spatial size, T is the temporal length, and $v_{i,j}[t]$ denotes the grayscale value of pixel (i, j) at time t , as follows:

$$\hat{v}_{i,j}[t] = \frac{v_{i,j}[t] - \mu_{i,j}}{\sigma}. \quad (9)$$

Above, $\mu_{i,j}$ denotes the empirical mean pixel value across time for the spatial location (i, j) , and σ denotes the empirical standard deviation across all pixels in one video. The subtraction of the mean emphasizes a subject’s local dynamics, while the division by the empirical standard deviation compensates for the variability in subject’s clothing.

Optical flow. As discussed earlier, we use a stacked block of optical flow frames as input to the temporal stream. We follow [28] and use colored optical flows. First, we compute optical flow between two consecutive normalized RGB frames [12]. The computed optical flow vectors are then mapped into polar coordinates and converted to hue and saturation based on the magnitude and orientation, respectively. The brightness is set to one. As a reminder, the eLR optical flows are computed on the interpolated 32×32 pixel eLR frames. Further, we subtract the mean of the stacked optical flows to compensate for global motion as suggested in [20].

4. Experiments

4.1. Datasets

In order to confirm the effectiveness of our proposed method, we conducted experiments on two publicly-available video datasets. First, we use the ROI sequences from the multi-view IXMAS action dataset, where each subject occupies most of the field of view [27]. This dataset includes 5 camera views, 12 daily-life motions each performed 3 times by 10 actors in an indoor scenario. Overall, it contains 1,800 videos. To generate the eLR videos (thus eLR-IXMAS), we decimated the original frames to 16×12 pixels and then upscaled them back to 32×32 pixels by bi-cubic interpolation (Fig. 4). The upscaling operation does not introduce new information (fundamentally, we are still working with 16×12 px) but ensures that eLR frames have enough spatial support for hierarchical convolutions to facilitate filter sharing. On the other hand, we generate the HR data by decimating the original frames straight to 32×32 pixels. We perform *leave-person-out* cross validation in each case and compute correct classification rate

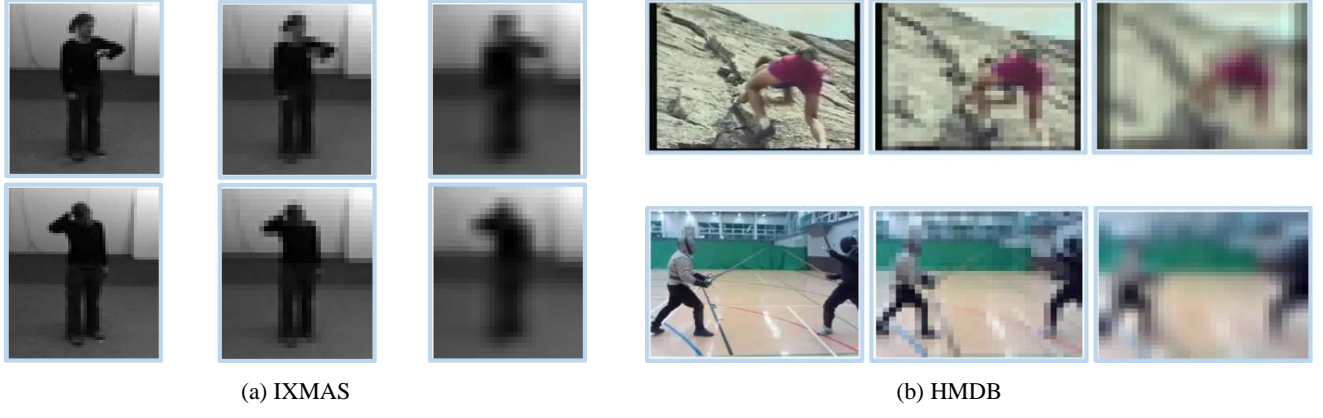


Figure 4: Sample frames from IXMAS and HMDB datasets. (a) From left to right are original frames, and resized 32×32 and 16×12 frames from the IXMAS dataset. (b) From left to right are original frames, and resized 32×32 and 12×16 frames from the HMDB dataset. Note that we resize the IXMAS dataset to 16×12 and the HMDB dataset to 12×16 in order to preserve the original aspect ratio. We use 32×32 resized videos as HR data. The 16×12 (12×16) eLR videos are upscaled using bi-cubic interpolation to 32×32 interpolated-eLR video which is used in our proposed semi-coupled fused two-stream ConvNet architecture.

(CCR) and standard deviation (StDev) to measure performance.

We also test our algorithm on the popular HMDB dataset [10] used for video activity recognition. The HMDB dataset consists of 6,849 videos divided into 51 action categories, each containing a minimum of 101 videos. In comparison to IXMAS, which was collected in a controlled environment, the HMDB dataset includes clips from movies and YouTube videos, which are not limited in terms of illumination and camera position variations. Therefore, HMDB is a far more challenging dataset, especially when we decimate to eLR, which we herein refer to as eLR-HMDB. In our experiments, we used the three training-testing splits provided with this dataset. Note that since there are 51 classes in the HMDB dataset, the CCR based on a purely random guess is 1.96%.

4.2. Results for eLR-IXMAS

We first conduct a detailed evaluation of the proposed paradigms on the eLR-IXMAS action dataset. For a fair comparison, we follow the image resolution, pre-processing and cross-validation as described in [3]. We first resize all video clips to a fixed temporal length $T = 100$ using cubic-spline interpolation.

Table 1 summarizes the action recognition accuracy on the eLR-IXMAS dataset. We report the CCR for separate spatial and temporal ConvNets, as well as for various locations and operators of fusion, with and without eLR-HR coupling. We also report the baseline result from [3] which employs a nearest-neighbor classifier.

We first observe that dedicated spatial or temporal ConvNet outperforms the benchmark result from [3] by 8.6%

Table 1: Performance of different ConvNet architectures against baseline on the eLR-IXMAS dataset. “Spatial & temporal average” has been performed by averaging the temporal and spatial stream predictions. The best performing method is highlighted in bold.

| Method | Fusion Layer | eLR-HR coupling? | CCR | StDev |
|----------------------|--------------|------------------|--------------|-------------|
| Baseline (Dai [3]) | - | - | 80.0% | 6.9% |
| Spatial Network | - | No | 88.6% | 6.2% |
| Temporal Network | - | No | 91.6% | 4.9% |
| Spatial&Temporal avg | Softmax | No | 92.0% | 6.0% |
| Concat Fusion | Fc 4 | No | 92.2% | 5.2% |
| | Fc 4 | Yes | 92.5% | 5.5% |
| | Conv 3 | No | 92.2% | 5.2% |
| | Conv 3 | Yes | 93.3% | 5.6% |
| Conv Fusion | Fc 4 | No | 92.0% | 5.8% |
| | Fc 4 | Yes | 93.1% | 5.2% |
| | Conv 3 | No | 93.3% | 4.0% |
| | Conv 3 | Yes | 93.7% | 4.5% |
| Sum Fusion | Fc 4 | No | 92.2% | 5.5% |
| | Fc 4 | Yes | 92.8% | 7.1% |
| | Conv 3 | No | 93.0% | 4.7% |
| | Conv 3 | Yes | 93.6% | 4.0% |

and 11.6% respectively, which validates the discriminative power of a ConvNet. If we equally weigh these two streams, as shown in “Spatial & Temporal avg”, we can see that

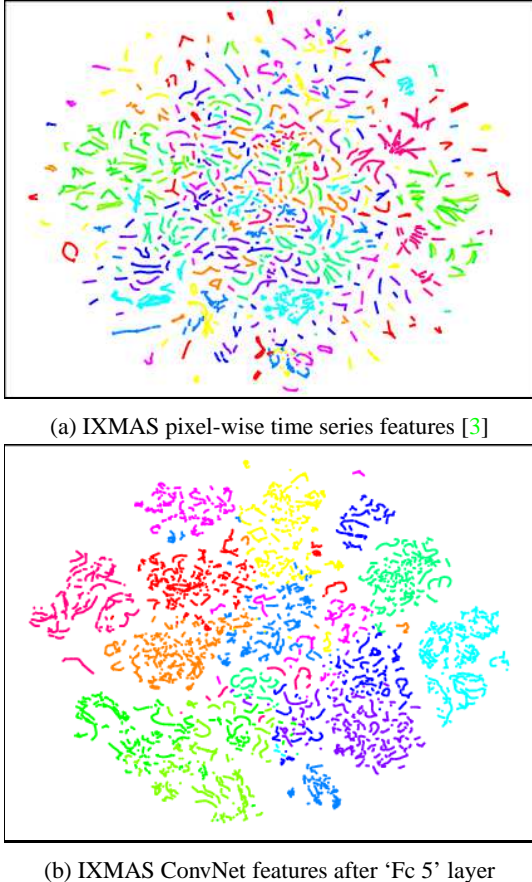


Figure 5: 2-D t-SNE embeddings [14] of features for the eLR-IXMAS dataset. A single marker represents a single video clip and is color-coded by action type. (a) Embeddings of pixel-wise time series features [3]. (b) Embeddings of the last fully-connected layer’s output from our best performing ConvNet.

fusion only marginally improves recognition performance. Secondly, we can see that fusing after the “Conv3” layer consistently provides better performance than fusing after the “Fc4” layer. In our preliminary experiments, we also found that fusing after the “Conv3” layer was consistently better than fusing after the “Conv2” layer, which suggests that there is an ideal depth (which is not too shallow or too deep in the network) for fusion. Regarding which fusion operator to use, we note that all 3 operators we consider provide comparable performance after the “Fc4” layer. However, if we fuse after the “Conv3” layer, convolutional fusion performs best.

As for the effectiveness of semi-coupling in the networks using HR information, we can see that eLR-HR coupling consistently improves recognition performance. Our best result on IXMAS is 93.7%, where we find that without coupling, our performance drops by 0.4%. This result is very

Table 2: Comparison of the number of parameters of our best performing action recognition ConvNet as compared to those of the standard-resolution image classification ConvNets.

| Network | No. of parameters |
|---------|-------------------|
| Ours | 0.84M |
| AlexNet | 60M |
| VGG-16 | 138M |
| VGG-19 | 144M |

close to that achieved by using *only* HR data in both training and testing, which is 94.4% CCR. Effectively, this should be an upper-bound, in terms of performance, when using eLR-HR coupling in training but testing *only* on eLR data. That the performance gap between HR and eLR is small may be explained by the distinctiveness of actions and the controlled indoor environment (static cameras, constant illumination, etc.) in the IXMAS dataset. Additionally, the fine details (e.g., hair, facial features) that are only visible in HR are not critical for action recognition.

In order to qualitatively evaluate our proposed model, we visualize various feature embeddings for the eLR-IXMAS dataset. We extract output features of the “Fc5” layer from the best-performing ConvNet (shown in bold), and project them to 2-dimensional space using t-SNE [14]. For comparison, we also apply t-SNE to the pixel-wise time series features proposed in our benchmark [3]. As seen in Fig. 5, the feature embedding from our ConvNet model is visually more separable than that of our baseline. This is not surprising, as we are able to consistently outperform the baseline on the eLR-IXMAS dataset.

Regarding the number of parameters, our ConvNet designed for eLR videos needs about 100 times less parameters than state-of-the art ConvNets like AlexNet [9], VGG-16, and VGG-19 [21] (Table 2). In consequence, this significantly reduces the computation cost of training and testing compared to these standard-resolution networks..

4.3. Results for eLR-HMDB

We also report the results of our methods on eLR-HMDB. Note that, for this dataset, we only report results for fusion after the “Conv3” layer, based on our observations from eLR-IXMAS. We follow the same pre-processing procedure as used for eLR-IXMAS except that we do not resize the video clips temporally for the purpose of having a fair comparison with the results reported in [17]. Our reported CCR is an average across the three training-testing splits provided with this dataset.

First, we measure the performance of a dedicated spatial-stream ConvNet and a dedicated temporal-stream ConvNet.

As shown in Table 3, only using appearance information (the spatial stream) provides 19.1% accuracy. If optical flow is used alone (the temporal stream), performance drops to 18.3%. This is likely because the videos in HMDB are unconstrained, as camera movement is not guaranteed to be well-behaved, thus resulting in drastically different optical flow quality across videos. Such variations are likely to be amplified in eLR videos. We then evaluate the same three fusion operators after the “Conv3” layer. Not surprisingly, compared to the average of predictions from a dedicated spatial network and a dedicated temporal network, fusing the temporal and spatial streams improves the recognition performance by 0.8%, 0.9% and 1.8% with concatenation, convolution, and sum fusion, respectively.

Table 3: Performance of different ConvNet architectures and current state-of-the-art method on the eLR-HMDB dataset. The two-stream networks are all fused after the “Conv3” layer. The best method is highlighted in bold.

| Method | eLR-HR coupling? | CCR |
|---|------------------|--------------|
| Spatial Network | No | 19.1% |
| Temporal Network | No | 18.3% |
| Spatial & Temporal avg | No | 19.6% |
| Concat Fusion | No | 20.4% |
| | Yes | 27.1% |
| Conv Fusion | No | 20.5% |
| | Yes | 27.3% |
| Sum Fusion | No | 21.4% |
| | Yes | 29.2% |
| ConvNet feat + SVM[17] | - | 18.9% |
| ConvNet feat + ISR + SVM[17] | - | 20.8% |
| ConvNet + hand-crafted feat + ISR + SVM[17] | - | 28.7% |

eLR-HR coupling can be shown to greatly enhance recognition performance. We achieve large performance gains from 20.4% to 27.1% using concatenation fusion, 20.5% to 27.3% using convolutional fusion, and 21.4% to 29.2% using sum fusion. Such notable improvements validate the discriminative capabilities of semi-coupled fused two-stream ConvNets. Compared to the state-of-the-art results reported in [17], our approach is able to outperform their ConvNet feature-only method by 8.4%. We also exceed the performance of their best method, that uses an augmented hand-crafted feature vector, by 0.5%.

5. Conclusion

In this paper, we proposed multiple, end-to-end ConvNets for action recognition from extremely low resolution videos (e.g. 16×12 pixels). We proposed multiple eLR ConvNet architectures, each leveraging and fusing spatial and temporal information. Further, in order to leverage HR videos in training we incorporated eLR-HR coupling to learn an intelligent mapping between the eLR and HR feature spaces. The effectiveness of this architecture has been validated on two datasets. We achieved superior results to state-of-the-art on the eLR-IXMAS and the eLR-HMDB datasets.

References

- [1] R. Chaudhry, A. Ravichandran, G. Hager, and R. Vidal. Histograms of oriented optical flow and binet-cauchy kernels on nonlinear dynamical systems for the recognition of human actions. In *Computer Vision and Pattern Recognition, 2009. CVPR 2009. IEEE Conference on*, pages 1932–1939. IEEE, 2009. [2](#)
- [2] J. Chen, J. Wu, K. Richter, J. Konrad, and P. Ishwar. Estimating head pose orientation using extremely low resolution images. In *2016 IEEE Southwest Symposium on Image Analysis and Interpretation (SSIAI)*, pages 65–68. IEEE, 2016. [1](#)
- [3] J. Dai, J. Wu, B. Saghafi, J. Konrad, and P. Ishwar. Towards privacy-preserving activity recognition using extremely low temporal and spatial resolution cameras. In *Proceedings of the IEEE Conference on Computer Vision and Pattern Recognition Workshops*, pages 68–76, 2015. [1, 2, 6, 7](#)
- [4] N. Dalal and B. Triggs. Histograms of oriented gradients for human detection. In *2005 IEEE Computer Society Conference on Computer Vision and Pattern Recognition (CVPR’05)*, volume 1, pages 886–893. IEEE, 2005. [2](#)
- [5] C. Feichtenhofer, A. Pinz, and A. Zisserman. Convolutional two-stream network fusion for video action recognition. In *The IEEE Conference on Computer Vision and Pattern Recognition (CVPR)*, June 2016. [1, 2, 3](#)
- [6] X. Glorot, A. Bordes, and Y. Bengio. Domain adaptation for large-scale sentiment classification: A deep learning approach. In *Proceedings of the 28th International Conference on Machine Learning (ICML-11)*, pages 513–520, 2011. [5](#)
- [7] S. Ji, W. Xu, M. Yang, and K. Yu. 3d convolutional neural networks for human action recognition. *IEEE transactions on pattern analysis and machine intelligence*, 35(1):221–231, 2013. [2](#)
- [8] A. Karpathy, G. Toderici, S. Shetty, T. Leung, R. Sukthankar, and L. Fei-Fei. Large-scale video classification with convolutional neural networks. In *Proceedings of the IEEE conference on Computer Vision and Pattern Recognition*, pages 1725–1732, 2014. [2](#)
- [9] A. Krizhevsky, I. Sutskever, and G. E. Hinton. Imagenet classification with deep convolutional neural networks. In *Advances in neural information processing systems*, pages 1097–1105, 2012. [1, 7](#)

[10] H. Kuehne, H. Jhuang, E. Garrote, T. Poggio, and T. Serre. Hmdb: a large video database for human motion recognition. In *2011 International Conference on Computer Vision*, pages 2556–2563. IEEE, 2011. 6

[11] T.-Y. Lin, A. RoyChowdhury, and S. Maji. Bilinear cnn models for fine-grained visual recognition. In *Proceedings of the IEEE International Conference on Computer Vision*, pages 1449–1457, 2015. 1, 2, 3

[12] C. Liu. *Beyond pixels: exploring new representations and applications for motion analysis*. PhD thesis, Citeseer, 2009. 5

[13] Y. M. Lui, D. Bolme, B. A. Draper, J. R. Beveridge, G. Givens, P. J. Phillips, et al. A meta-analysis of face recognition covariates. *Biometrics: Theory, Applications, and Systems*, pages 1–8, 2009. 3

[14] L. v. d. Maaten and G. Hinton. Visualizing data using t-sne. *Journal of Machine Learning Research*, 9(Nov):2579–2605, 2008. 7

[15] E. Park, X. Han, T. L. Berg, and A. C. Berg. Combining multiple sources of knowledge in deep cnns for action recognition. In *2016 IEEE Winter Conference on Applications of Computer Vision (WACV)*, pages 1–8. IEEE, 2016. 1, 2

[16] D. Roeperi, J. Chen, A. Greco, J. Konrad, and P. Ishwar. Privacy-preserving, indoor occupant localization using a network of single-pixel sensors. In *Advanced Video and Signal Based Surveillance (AVSS), 2016 13th IEEE International Conference on*, Aug 2016. 1

[17] M. S. Ryoo, B. Rothrock, and C. Fleming. Privacy-preserving egocentric activity recognition from extreme low resolution. *arXiv preprint arXiv:1604.03196*, 2016. 1, 2, 7, 8

[18] M. S. Ryoo, B. Rothrock, and L. Matthies. Pooled motion features for first-person videos. In *Proceedings of the IEEE Conference on Computer Vision and Pattern Recognition*, pages 896–904, 2015. 2

[19] A. Sharif Razavian, H. Azizpour, J. Sullivan, and S. Carlsson. Cnn features off-the-shelf: an astounding baseline for recognition. In *Proceedings of the IEEE Conference on Computer Vision and Pattern Recognition Workshops*, pages 806–813, 2014. 1

[20] K. Simonyan and A. Zisserman. Two-stream convolutional networks for action recognition in videos. In *Advances in Neural Information Processing Systems*, pages 568–576, 2014. 1, 2, 5

[21] K. Simonyan and A. Zisserman. Very deep convolutional networks for large-scale image recognition. *CoRR*, abs/1409.1556, 2014. 1, 7

[22] D. Tran, L. Bourdev, R. Fergus, L. Torresani, and M. Paluri. C3d: generic features for video analysis. *CoRR*, abs/1412.0767, 2:7, 2014. 2

[23] A. Vedaldi and K. Lenc. Matconvnet: Convolutional neural networks for matlab. In *Proceedings of the 23rd ACM international conference on Multimedia*, pages 689–692. ACM, 2015. 5

[24] H. Wang and C. Schmid. Action recognition with improved trajectories. In *Proceedings of the IEEE International Conference on Computer Vision*, pages 3551–3558, 2013. 1

[25] W. Wang, Z. Cui, H. Chang, S. Shan, and X. Chen. Deeply coupled auto-encoder networks for cross-view classification. *arXiv preprint arXiv:1402.2031*, 2014. 5

[26] Z. Wang, S. Chang, Y. Yang, D. Liu, and T. S. Huang. Studying very low resolution recognition using deep networks. In *The IEEE Conference on Computer Vision and Pattern Recognition (CVPR)*, June 2016. 1, 2, 3, 4, 5

[27] D. Weinland, M. Özysal, and P. Fua. Making action recognition robust to occlusions and viewpoint changes. In *European Conference on Computer Vision*, 2010. 5

[28] J. Wu, P. Ishwar, and J. Konrad. Two-stream cnns for gesture-based verification and identification: Learning user style. In *The IEEE Conference on Computer Vision and Pattern Recognition (CVPR) Workshops*, June 2016. 5

[29] L. Xia, C.-C. Chen, and J. Aggarwal. View invariant human action recognition using histograms of 3d joints. In *2012 IEEE Computer Society Conference on Computer Vision and Pattern Recognition Workshops*, pages 20–27. IEEE, 2012. 1